EFFECTS OF PARTICLES' MIXING AND SCATTERING IN THE DUSTY GAS FLOW THROUGH THE MOVING AND STATIONARY CASCADES OF AIRFOILS

Yu.M. Tsirkunov, D.A. Romanyuk and S.V. Panfilov

Baltic State Technical University, Faculty of Aerospace Engineering
1st Krasnoarmeiskaya str. 1, 190005 Saint Petersburg, Russia
E-mail: tsrknv@bstu.spb.su

ABSTRACT

Time-dependent 2D-flow of dusty gas through a set of two cascades of airfoils (blades) is studied numerically. The first cascade moves (rotor) and the second one is immovable (stator). Such a flow can be considered, in some sense, as a flow in an inlet stage of a turbomachine, for example, for an inlet compressor of an aircraft turbojet engine. The dust particles' concentration is assumed to be very low, so that the inter-particle collisions and effect of the dispersed phase on the carrier gas are negligible. Flow of the carrier gas is described by the complete Navier–Stokes equations. In calculations of the particles' motion, they were assumed to be solid spheres. The particle drag force, the transverse Magnus force, and the damping torque are taken into account in the model of gas–particle interaction. Impact interaction of particles with blades is considered as frictional and not completely elastic. The effects of particles' distribution in size and the particles' scattering in particle–blade collisions are investigated. Flow fields of the carrier gas and the flow patterns of the particle phase are obtained and discussed.

1. INTRODUCTION

Flow through cascades of airfoils occurs in aircraft turbojet engines and other axial turbomachines. In practice, a working gas flowing through a machine channel often contains suspended solid particles or liquid droplets. The presence of a dispersed phase in the flow results in some new effects which more often than not, are undesirable. Specifically, it causes the erosion of blades due to multiple impacts of particles or droplets with them and the additional momentum and energy losses [1]. In this case, one of important problems is the protection of blades and other parts of a channel from erosion. The most vulnerable to particles' "attack" is an inlet stage of a turbomachine. With application to an aircraft turbojet engine (see Fig. 1) it is an inlet compressor. For prediction of areas on blade surfaces which are exposed to the strongest erosive effect, it is necessary to have a clear insight into of characteristic features of particles' behaviour in the flow. Actual flow in a turbomachine channel is, strictly speaking, three-dimensional. The 3D-effects are particularly essential near the axis and near the channel walls. However, some important flow features in the inlet stage and in the sequential rims can be studied with the use of 2D-flow model in the plane, which represents a developed mean circle cross-section (see Fig. 2). Such an approach turned out very fruitful and brought the well-known 2D-theory of cascade flow into being (e.g., [2]). This theory deals with steady-state dust-free gas flows. Steady-state flow of gas-particle mixture through an immovable cascade was analyzed by Hussein & Tabakoff [3]. Steady-state gas-particle flow approximation was used in [4] to study the flow in a single rotating cascade.

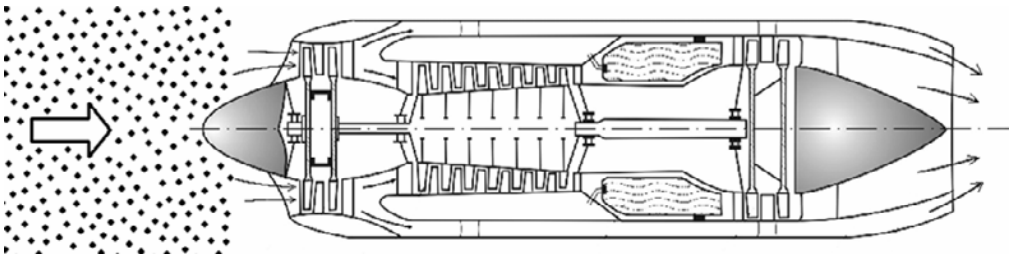

Fig. 1. Dusty gas flow through an aircraft turbojet engine.

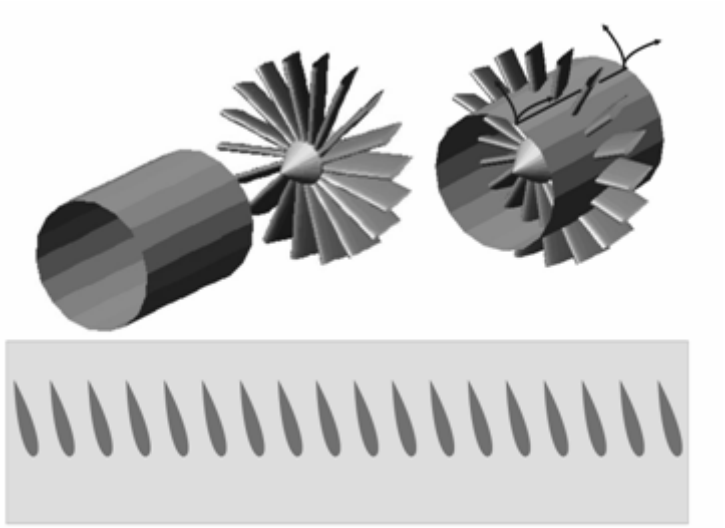

Fig. 2. Scheme of going from 3D-configuration of a rim of blades to 2D-configuration of a cascade of airfoils.

In the present study the behaviour of solid particles in the time-dependent high-speed subsonic 2D-flow in a set of two, moving and stationary, cascades of blades is simulated numerically and analyzed. The particle mass load is assumed to be very low, so that the inter-particle collisions and the effect of the dispersed phase on the carrier gas flow can be neglected. In this case, the problem of two-phase flow simulation is reduced to the sequential solving of two problems: (i) computation of the carrier gas flow field, and (ii) calculation of the particles' motion in this flow field. The input data in computations (flow properties, speed of the moving cascade, airfoil sizes, *etc*.) were taken close to those in the flow through an axial compressor of an aircraft turbojet engine. The main aim of this study is to understand how such actual effects as the particles' distribution in size and the scattering of particles in particle–blade collisions influence the particle phase flow structure in a complex flow of dusty gas through the inlet system "rotor–stator" of a turbojet engine.

2. FORMULATION OF THE PROBLEM AND NUMERICAL METHOD

2.1. Schematic of flow

We consider a two-phase gas–particle flow though a set of two cascades, the first of which moves with the constant velocity V_r and the second one is stationary (see Fig. 3). Both cascades have the same step s (distance between airfoils along a cascade). Airfoils of the first cascade are set at angle β with respect to the undisturbed flow direction. For visualization of the particle-phase flow in computational simulation, particles from a cloud of finite width h equal to the airfoil chord l were considered.

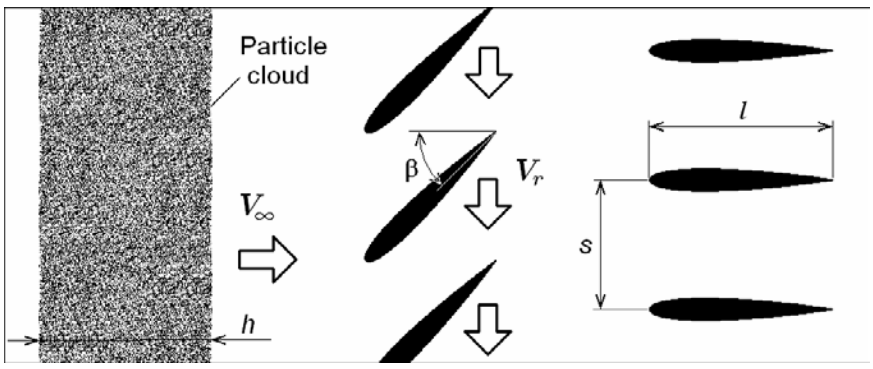

Fig. 3. Schematic of arrangement of the two cascades in an undisturbed flow.

Under the above assumptions a two-phase flow can be considered as one-way coupled and dilute. Estimates for the particle concentration when this model is valid were obtained in [5]. They show that the upper bound of the concentration depends on the particle size, all other parameters being fixed. Motion of particles is governed by the gas–particle interaction and the particle–airfoil collisions. Particles being more inertial compared with the carrier gas do not follow streamlines and they can collide with airfoils and rebound from them. Trajectories of rebounded (reflected) particles can intersect with each other and with the ones of incident particles. Calculations of a large number of particles allow an understanding of specific features of particles' behaviour in the flow. Because the gas–particle flow considered in the present study is time-dependent, instant flow patterns of the carrier gas and the particle phase will be given and discussed below.

2.2. Modelling of the carrier gas flow

The classical theory of cascades is based on the model of inviscid gas. Preliminary computational simulation of a high-speed subsonic gas flow through the "rotor–stator" set of cascades was performed on the basis of the Euler equations and the complete Navier–Stokes equations. The same grid was used in the computation domain in both cases. Comparison of the results showed that the effects associated with gas viscosity (development of boundary layers on airfoils and vortex wakes behind them) played an important role in forming the flow structure. The Reynolds number $\mathrm{Re}_\infty = \rho_\infty V_\infty l / \mu_\infty$ (l is the chord of an airfoil) in our problem is approximately equal to $1.4 \cdot 10^6$, hence, the flow is turbulent, and the conventional approach requires in this case to use the Reynolds averaged Navier–Stokes equations (or like that) instead of the Navier–Stokes equations by themselves. However, we share this judgment only in part. The matter is that the large-scale vortex flow structure, which is of greatest important in many applications, can be obtained very often without fine modelling of the turbulence and even without the boundary layer effects. In the present study a large-scale vortex street arises behind airfoils due to interaction of boundary layers separated run off airfoils. This effect will be best demonstrated by computational results in Section 3.

The Navier–Stokes equations for time-depended compressible 2D-flow can be written in Cartesian coordinates $(x,\ y)$ in the following compact form [6]:

$$\frac{\partial \mathbf{U}}{\partial t} + \frac{\partial \mathbf{F}_x}{\partial x} + \frac{\partial \mathbf{F}_y}{\partial y} = \frac{\partial \mathbf{G}_x}{\partial x} + \frac{\partial \mathbf{G}_y}{\partial y}, \tag{1}$$

where vectors $\mathbf{U}$, $\mathbf{F}_x$, $\mathbf{F}_y$, $\mathbf{G}_x$, and $\mathbf{G}_y$ are defined as follows

$$\mathbf{U} = \begin{pmatrix} \rho \\ \rho u \\ \rho v \\ \rho e \end{pmatrix}, \quad \mathbf{F}_x = \begin{pmatrix} \rho u \\ \rho u^2 + p \\ \rho uv \\ (\rho e + p)u \end{pmatrix}, \quad \mathbf{F}_y = \begin{pmatrix} \rho v \\ \rho uv \\ \rho v^2 + p \\ (\rho e + p)v \end{pmatrix}, \tag{2}$$

$$\mathbf{G}_x = \begin{pmatrix} 0 \\ \tau_{xx} \\ \tau_{xy} \\ u\tau_{xx} + v\tau_{xy} - q_x \end{pmatrix}, \quad \mathbf{G}_y = \begin{pmatrix} 0 \\ \tau_{xy} \\ \tau_{yy} \\ u\tau_{xy} + v\tau_{yy} - q_y \end{pmatrix}.$$

Here

$$p = \rho RT, \quad e = c_V T + \frac{u^2 + v^2}{2}, \quad q_x = -\lambda \frac{\partial T}{\partial x}, \quad q_y = -\lambda \frac{\partial T}{\partial y},$$

$$\tau_{xx} = \frac{2}{3}\mu\left(2\frac{\partial u}{\partial x} - \frac{\partial v}{\partial y}\right), \quad \tau_{yy} = \frac{2}{3}\mu\left(2\frac{\partial v}{\partial y} - \frac{\partial u}{\partial x}\right), \quad \tau_{xy} = \mu\left(\frac{\partial u}{\partial y} + \frac{\partial v}{\partial x}\right).$$

In the above equations, t is the time; ρ, p, e, T, μ, λ are the gas density, the pressure, the specific total energy, the temperature, the viscosity, and the thermal conductivity, respectively; u and v are the x- and y-components of the velocity vector; R is the specific gas constant, c_V is the specific heat at constant volume. In the present study the following relations for μ and λ are used

$$\mu = \mu_0 \left(\frac{T}{T_0} \right)^{3/2} \frac{T_0 + S_0}{T + S_0}, \qquad \lambda = \frac{c_p \mu}{\mathrm{Pr}},$$

where the first relation is the Sutherland formula, $\mu_0 = 1.71 \cdot 10^{-5}$ Ns/m^2, $T_0 = 288$ K, $S_0 = 117$ K, Pr is the Prandtl number, c_p is the specific heat at constant pressure.

The Navier–Stokes equations are solved numerically, and the boundary conditions with application to the computation domain will be described and discussed in subsection *2.4*.

2.3. Modelling of the particle phase flow

The Lagrangian approach is used for modelling of the particles' motion. The motion of a particle is described by the momentum and angular momentum equations which are added by the kinematic relation between the particle position vector $\mathbf{r}$ and the velocity vector $\mathbf{v}_\mathrm{p}$

$$m_\mathrm{p} \frac{d\mathbf{v}_\mathrm{p}}{dt} = \mathbf{f}_\mathrm{D} + \mathbf{f}_\mathrm{M}, \qquad J_\mathrm{p} \frac{d\boldsymbol{\omega}_\mathrm{p}}{dt} = \mathbf{L}_\mathrm{p}, \qquad \frac{d\mathbf{r}}{dt} = \mathbf{v}_\mathrm{p} \tag{3}$$

Here $m_\mathrm{p} = 4\rho_\mathrm{p}\pi r_\mathrm{p}^3 / 3$, $J_\mathrm{p} = 2 m_\mathrm{p} r_\mathrm{p}^2 / 5$, r_p, and $\boldsymbol{\omega}_\mathrm{p}$, are the particle mass, the moment of inertia, the radius, and the rotational velocity, respectively. We include into the force on a particle the drag force $\mathbf{f}_\mathrm{D}$ and the lift Magnus force $\mathbf{f}_\mathrm{M}$, which dominate over other components in the considered flow. The Magnus force is developed due to simultaneous translational and rotational motion of a particle, and it can be significant for particles twisted in particle–airfoil collisions. The damping torque $\mathbf{L}_\mathrm{p}$ acts on a particle if its relative rotational velocity is not zero. We use the conventional relations for calculation of $\mathbf{f}_\mathrm{D}$, $\mathbf{f}_\mathrm{M}$ and $\mathbf{L}_\mathrm{p}$

$$\mathbf{f}_\mathrm{D} = \frac{1}{2} C_\mathrm{D} \pi r_\mathrm{p}^2 \rho |\mathbf{v} - \mathbf{v}_\mathrm{p}| (\mathbf{v} - \mathbf{v}_\mathrm{p}),$$

$$\mathbf{f}_\mathrm{M} = \frac{4}{3} C_\omega \pi r_\mathrm{p}^3 \rho [(\boldsymbol{\omega} - \boldsymbol{\omega}_\mathrm{p}) \times (\mathbf{v} - \mathbf{v}_\mathrm{p})],$$

$$\mathbf{L}_\mathrm{p} = \frac{1}{2} C_L r_\mathrm{p}^5 \rho \, |\boldsymbol{\omega} - \boldsymbol{\omega}_\mathrm{p}| (\boldsymbol{\omega} - \boldsymbol{\omega}_\mathrm{p}), \qquad \boldsymbol{\omega} = \frac{1}{2} \mathrm{curl}\, \mathbf{v}.$$

The coefficients C_D, C_ω, and C_L depend on dimensionless flow parameters around a particle: the relative Mach and Reynolds numbers, the relative rotational Reynolds number, *etc*. These coefficients are calculated from approximate formulae which are constructed on the basis of theoretical solutions, numerical results and experimental data. We have used the Henderson relations [10] for C_D. For calculation of C_ω we have used the exact solution by Rubinow and Keller [11] or the formula suggested by Oesterlè and Bui Dinh [12]. The expression for C_L has been taken in the form suggested by Dennis *et. al*. [13].

For determination of the particle parameters just after its rebound from an airfoil surface, we use the *semi-empirical model* [7] *for spherical* particles and the *simplified model* with constant restitution coefficients for the normal and tangential components of the contact point velocity [8] *for non-spherical* particles. The semi-

empirical model is based on the mechanics laws and the experimental data on the restitution coefficients of the translational velocity components.

In the majority of papers on two-phase gas–particle flow, the particles are assumed to be rigid spheres of *the same radius* and *no scattering* in particle–wall collisions is taken into account. However in practice, particles are distributed in size that results in mixing of particles of different size in a disturbed flow. Second, the particles' shape is often differs from a sphere, and this results in their scattering in particle–wall collisions. In the present study we investigate the behaviour of polydisperse particles with the Log-normal distribution in size in an undisturbed flow, and also we take into account the scattering of particles due to their non-spherical shape. In the case of the Log-normal law, the particle mass frequency distribution function has the form

$$g_\infty(r_\mathrm{p}) = \frac{1}{\sqrt{2\pi}\, r_\mathrm{p} \log\sigma} \exp\left[-\left(\frac{\log r_\mathrm{p} - \log r_\mathrm{g}}{\sqrt{2}\, \log\sigma} \right)^2 \right]. \qquad (4)$$

Here the parameter r_g is correlated with the most probable particle size r_pm by $r_\mathrm{g} = r_\mathrm{pm}\exp(\log^2\sigma)$. The plot of function (4) for $\sigma = 1.2$ is shown in Fig. 4. For investigation of the effect of particle scattering we consider in the model of particle–wall collisions the particles with the shape of ellipsoids of revolution (Fig. 5). The ratio of axes b/a (a is the axis in ξ-direction, b is the axis in η- and ζ-direction) is taken close to a unity (0.8 and 1.25), so that the particle shape is close to sphere but does differ from it. A collision of a non-spherical particle with a wall is three-dimensional. The model of such collision and the scattering properties for particles of different shape are described in [8, 9]. In computational simulation of a particle–wall collision in the present study, the particle orientation in space just before a collision is considered as random with the assumption that the orientations of axes ξ, η and ζ relative to x, y, z are equiprobable. A particle just after a collision has three components of both, translational and rotational, velocities. However in simulation of the particle-phase flow we consider the reflected particles as spherical and take into account their scattering only in (x,y)-plane. Such an approach allows to understand whether the effect of scattering is of great importance or not, but the question of validation of the flow model remains open.

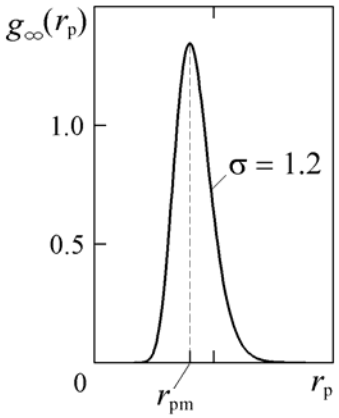

Fig. 4. Log-normal distribution.

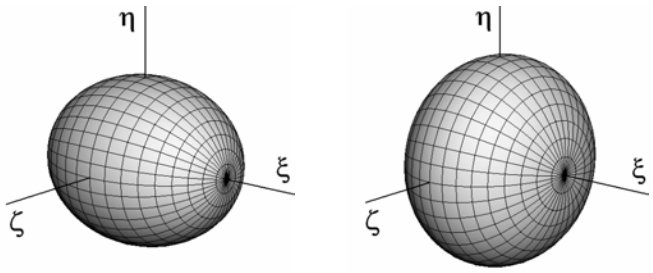

Fig. 5. Shape of particles in modelling of their scattering in particle–airfoil collisions: prolate with axes ratio 0.8 (left) and oblate with axes ratio 1.25 (right) ellipsoids of revolution.

2.4. Numerical method

Computation domain consists of two blocks (see Fig. 6). The left block moves together with a rotor blade, and right one is stationary. A structured curvilinear grid fitted to the blade contours is introduced in each block. Both grids are refined to the blade surfaces and in the areas behind blades to resolve the flow structure inside the boundary layers and in the wakes. The length of computation domain in the main flow direction is 4.4 l .

A finite-volume explicit in time method is used for numerical solving the Navier–Stokes equations (1). The "inviscid" fluxes $\mathbf{F}_x$ and $\mathbf{F}_y$ of conservative variables **U** (see Eq. (2)) through the cell faces are calculated by

the Roe scheme [14] with the use of the entropy correction suggested by Harten [15]. For calculation of the "viscous" fluxes $\mathbf{G}_x$ and $\mathbf{G}_y$, the reconstruction of gas parameters on the grid with taking into account their gradients inside every cell are used. The method used is of the second order in space. The time step is chosen from the conventional stability condition.

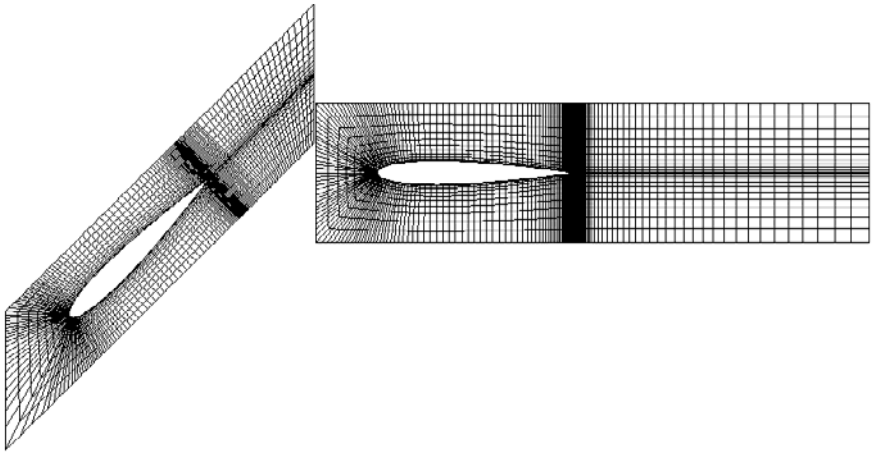

Fig. 6. Computational domain and schematic of a grid.

The periodic conditions in y-direction are set at the top and bottom boundaries of each block. This is possible if no large-scale areas of separated flow arise. A special matching procedure is used at the contact boundary between the moving and stationary blocks [16]. At the inflow boundary of the moving block, the velocity and density calculated from the given total enthalpy and entropy in the undisturbed flow are specified, and the pressure is extrapolated from the computation domain. At the outflow boundary of the stationary block, the pressure is taken equal to $1.2p_\infty$ (this value agrees with some experiments) and other parameters are extrapolated from the computation domain. Such a technique is in agreement with the characteristic properties of gas dynamic equations. At the airfoil surface, the no-slip condition and the constant-temperature wall condition are enforced.

A uniform flow with the undisturbed parameters is taken at the initial instant $t = 0$, and then computational simulations of the carrier gas flow is going on up to a quasi-time-periodic solution is reached. After this the particles are introduced into the simulation procedure.

The equations (3) for a particle are solved by a predictor–corrector method of the second order. Calculations are carried out simultaneously with the continuing solving of the Navier–Stokes equations. The total number of particles in a cloud is varied from 50,000 to 5,000,000.

3. RESULTS OF COMPUTATIONAL SIMULATION AND DISCUSSION

3.1. Input data

Parameters of the cascades and flow properties are taken in calculations close to those which are typical for an inlet compressor of a turbojet engine. The chord of airfoils is equal to l = 10 cm, the cascade step s = 7 cm, the angle of attack β = 45°, the profile of blades is NACA0012, the main (undisturbed) flow velocity V_∞ = 200 m/s, the cascade velocity V_r = 150 m/s, the carrier gas is air (R = 287 J/(kg K), c_p/c_V = 1.4), the Prandtl number Pr = 0.72, the flow density and temperature ρ_∞ = 1.21 kg/m^3 and T_∞ = 288 K. These values correspond to the Mach number M_∞ = 0.59. The particle and blade materials are SiO_2 and steel, respectively.

3.2. Results for the carrier gas

The majority of calculations of the carrier gas flow field were performed for the Navier–Stokes equations. However for comparison and for estimation of the "numerical scheme viscosity", calculations were also carried out

for the Euler equation using the same grids. Flow fields were obtained in both cases. The results for the entropy function $\theta = p/\rho^{\gamma}$ are shown in Fig. 7. It is clearly seen that in the case of the Euler equations we have nearly homogeneous entropy field that is in good agreement with the theoretical statement that the entropy in a flow of ideal gas remains constant. In the field of a viscous gas (Fig. 7, b) we see spots with much higher entropy than in the main stream. These inhomogeneities arise due to the entropy production in boundary layers at the blade surfaces and inside separated eddies in the vortex wakes behind blades. The structure of wakes is similar to that of the von Karman vortex street. Flow in both cases is subsonic in the stationary system of coordinates. In the outlet boundary of the calculation domain (right boundary of the stationary grid block), the gas velocity, the density, and the temperature reach nearly constant values: V = 115 m/s, ρ = 1.56 kg/m^3, T = 304 K. These parameters correspond to the Mach number M = 0.33.

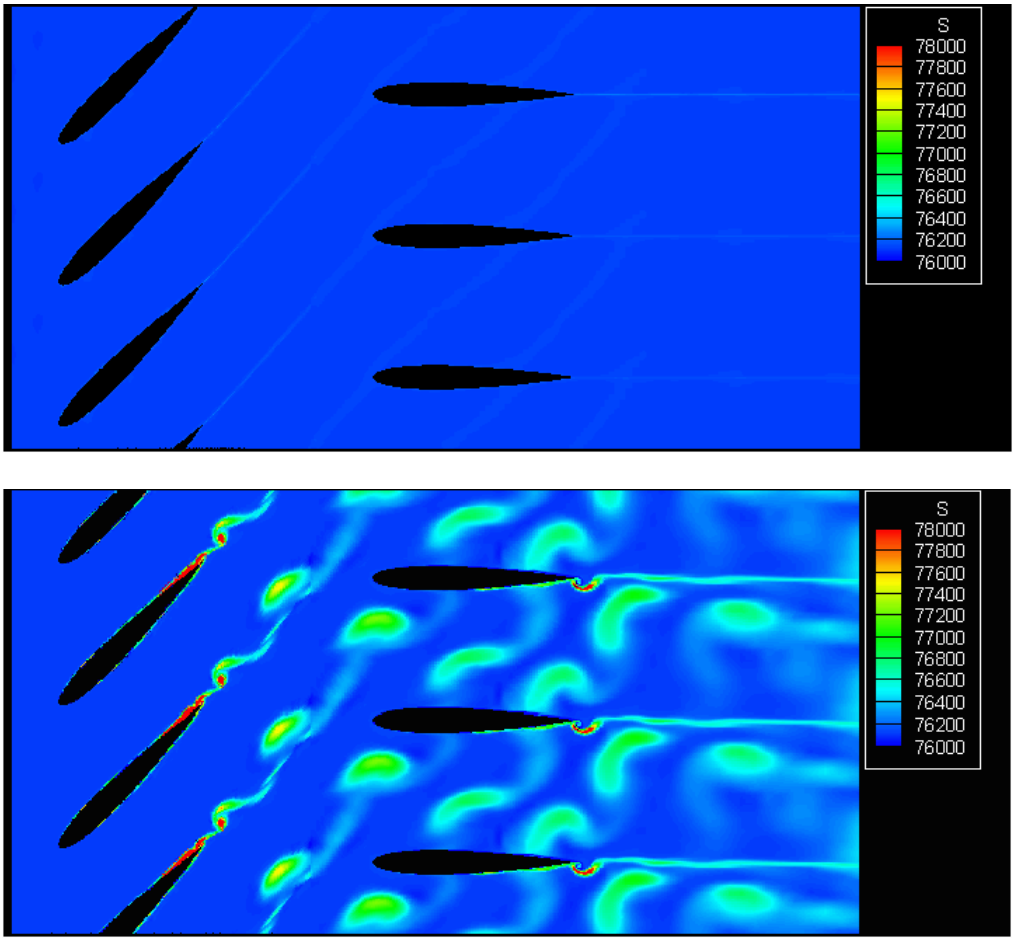

Fig. 7. Instant field of the entropy function $\theta = p/\rho^{\gamma}$ in the carrier gas flow: computation of the Euler (a) and Navier–Stokes (b) equations.

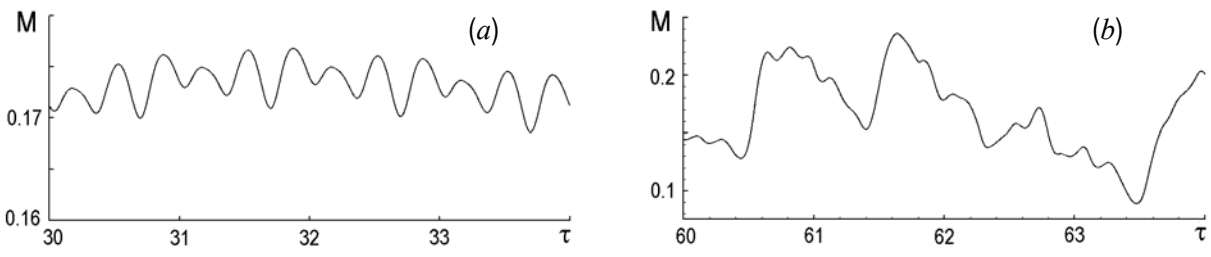

Fig. 8. Mach number in front of a stator airfoil as a function of time: computation of the Euler (a) and Navier–Stokes (b) equations.

The computational experiments have shown that numerical solution of the Euler equations reaches with time a strictly periodic behaviour that is illustrated by Fig. 8, *a*. In the figure $\tau = t/t_s$, where $t_s = s/V_r$ ($t_s = 0.47 \cdot 10^{-3}$ s for the given values of s and V_r). The period includes three maximums and three minimums. For the Navier–Stokes equations, the time-dependent character of a solution is illustrated by Fig. 8, *b*. It is seen that in this case a time-periodic solution is absent. Such a situation is connected with two independent periodic in time processes: separation of eddies from blades, and motion of spatially periodic rotor blades relative to the stator blades with the same spatial period. The first process is determined by the Reynolds number of flow around a blade, whereas the second one is determined by the velocity V_r and the cascade step s. If the periods of both processes are not multiple, their interaction can result in "stochastic" behaviour of flow parameters with time.

3.3. Results for the particle-phase

For visualization of the particle-phase flow we consider a particle cloud of finite width *h* in an undisturbed flow (see Fig. 1). In calculations *h* was taken equal to *l*. Particles in the cloud were distributed in space randomly by the uniform distribution. The below results were obtained for the carrier gas flow field computed from the Navier–Stokes equations. Instant particle flow patterns at the same moment are shown in Figs. 9 – 11. Particle radiuses r_p = 5 μm, 10 μm and 20 μm correspond to the Stokes numbers Stk = 1.70, 6.82 and 27.28, respectively. The Stokes number is defined as the ratio of the particle dynamic relaxation length (with the use of the Stokes law for a particle drag force) to the characteristic length in the flow *l*: Stk = $2\rho_p r_p^2 V_\infty / (9\mu_\infty l)$.

Figure 9 illustrates the dependence of flow structure of *monosized spherical* particles on their radius. A cloud stretches in the flow, and the distribution of particles in space becomes strongly non-uniform. Narrow layers with high particle concentration are clearly discernible. Such a redistribution of particles occurs by the

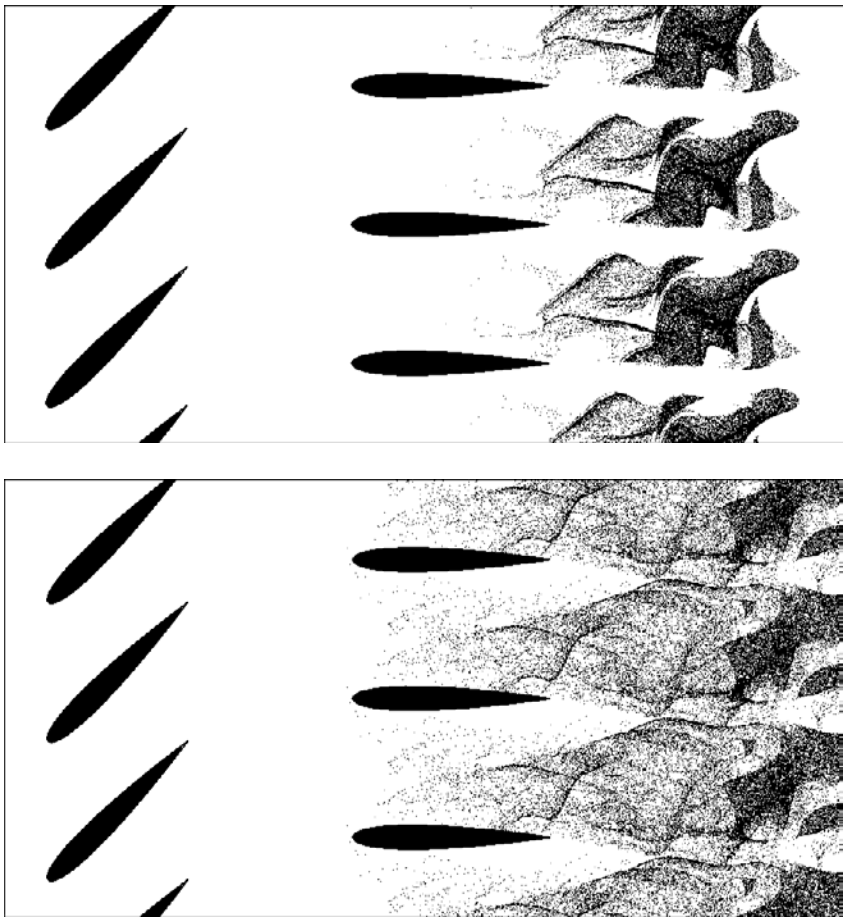

Fig. 9. For caption see next page.

(*c*)

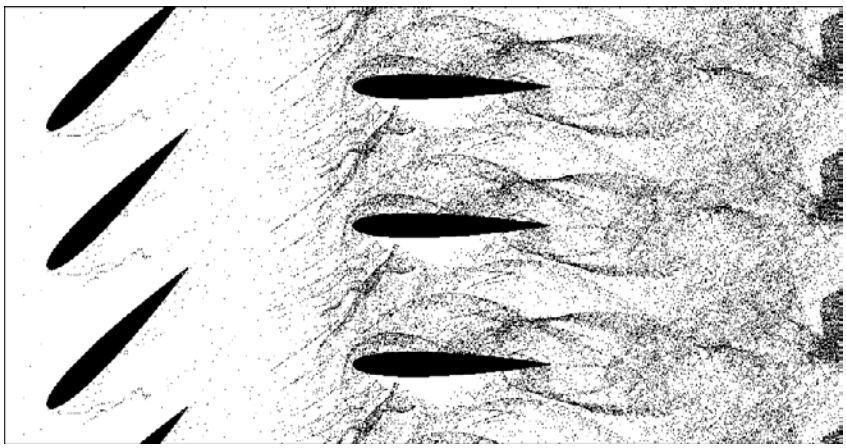

Fig. 9. Instant patterns of monosized spherical particles depending on the particle radius: r_p = 5 μm (*a*), 10 μm (*b*), 20 μm (*c*); a semi-empirical model of particle–wall collisions [7] is used.

action of non-uniform flow field of the carrier gas. For small particles (Stk < 10) the effect of boundary layers and vortex wakes is of great importance in the process of redistribution. For large particles (Stk > 20), this effect is negligible, but the particle–blade collisions play a key role.

Instant patterns of spherical particles log-normally distributed in size in an initial cloud are shown in Fig. 10. One can see also a strong redistribution of particles in the flow, but in this case, in contrast to Fig. 9, narrow layers with high particle concentration disappear. Thus, the polydispersity of the particle phase results in "smearing" of the concentration field. The physical reason of this effect is mixing of particles of different sizes in a flow.

(*a*)

(*b*)

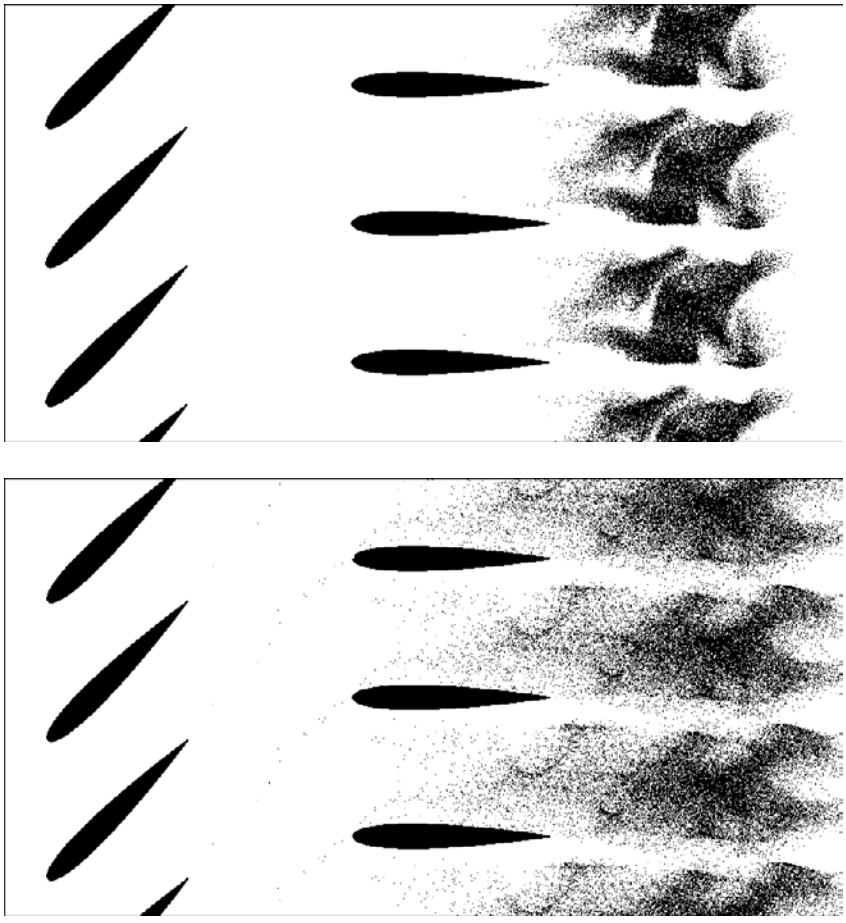

Fig. 10. For caption see next page.

(*c*)

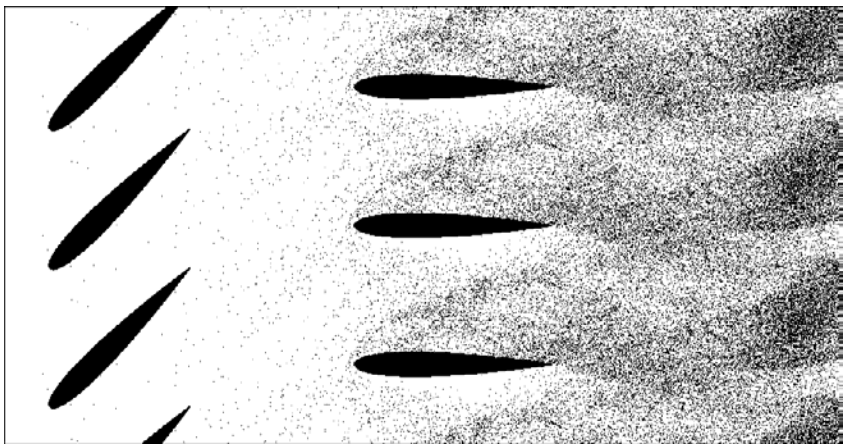

Fig. 10. Instant patterns of polydisperse spherical particles (Log-normal law (4) with σ =1.2 is taken in an initial cloud) depending on the most probable particle size: r_{pm} = 5 μm (*a*), 10 μm (*b*), 20 μm (*c*); a semi-empirical model of particle–wall collisions [7] is used.

Consider now the effect of particle scattering in particle–blade collisions due to non-spherical particles' shape and the joint effect of scattering and mixing. In this part of the study we assume particles to be solid spheres in calculation of their moving in the flow, but we consider them as ellipsoids in collisions with blades. The collision model for non-spherical particles tested for validity, to the authors' knowledge, is absent now, that is why a simplified collision model is used here. The restitution coefficients of the normal (a_{Cn}) and tangential ($a_{C\tau}$) velocities of the particle contact point are assumed to be constant. We take a_{Cn} = 0.8 and $a_{C\tau}$ = 0.

(*a*)

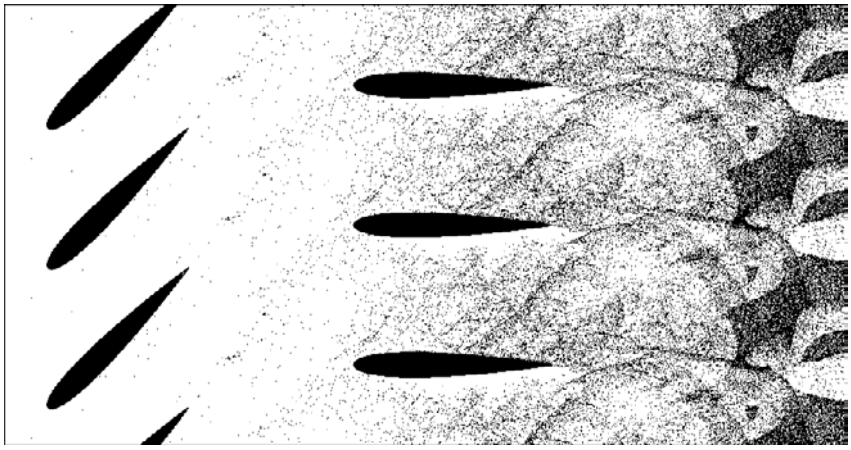

(*b*)

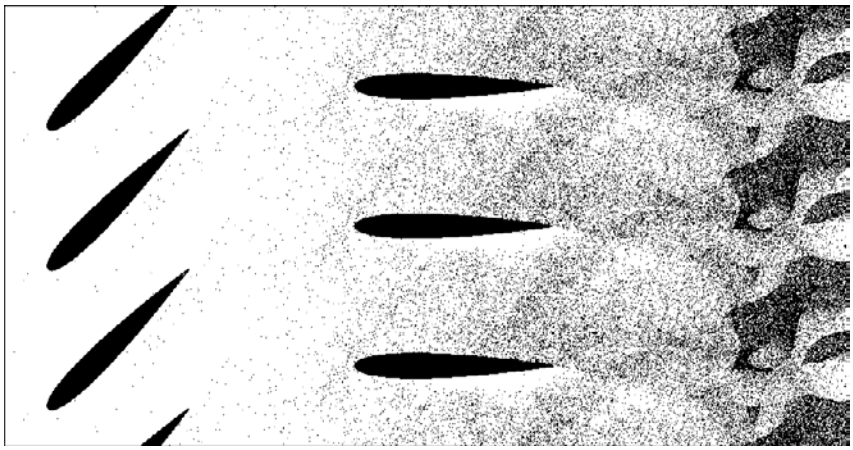

Fig. 11. For caption see next page.

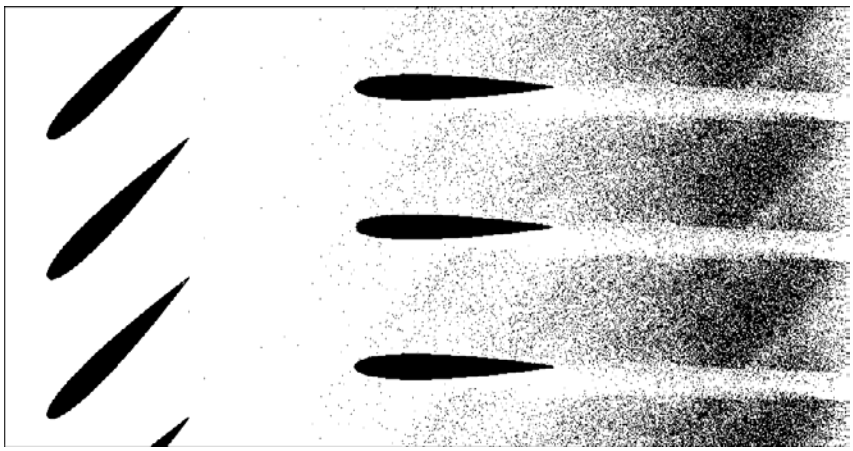

Fig. 11. Instant patterns of particles: monosized spherical particles of radius r_p = 10 μm (a); effect of scattering in particle–wall collisions (b); joint effect of scattering and mixing (c): Log-normal law (4) with σ =1.2 is taken in an initial cloud.

This means that we consider a non-completely elastic and non-sliding collision. This model was used also for spherical particles the motion of which was calculated for comparison. The results for the case of prolate ellipsoids (see Fig. 5, a) are shown in Fig. 11. It is seen from the figures (a) and (b) that the effect of particle scattering is similar to that of mixing discussed above: the particle concentration field becomes smearing. However, the joint effect of scattering and mixing is found to be unexpected at the first glance (cf. figures (b) and (c)). This result can be explained by a substantial increase of a number of small particles in a polydisperse mixture. Small particles follow the gas flow more closely than the large ones, and the majority of them do not collide with blades, so that the effect of scattering decreases in this case.

4. CONCLUDING REMARKS

The present investigation of dusty gas flow through a set "rotor–stator" of 2D-cascades has shown that dispersed particles are redistributed strongly in the flow. The behaviour of the particle phase depends substantially on the particle size. Motion of small particles is governed mainly by the carrier gas flow which is rather complicated due to separation of eddies from blades with forming the vortex wakes. Large particles colliding with the blades rebound from them and the rebounded particles can collide later with both, nearest and far blades, that makes the particle phase flow more complicated. In the case of monosized spherical particles, the narrow layers with high particle concentration arise. Mixing of particles of different sizes and particles' scattering due to their non-spherical shape result in smearing of these layers. This allow us to conclude that in actual dusty gas flows the erosive damage from the particles' impacts is less that it can be predicted by the classical two-phase flow theory assuming the particles to be spheres of the same radius.

ACKNOWLEDGEMENTS

This study was supported by the Russian Foundation for Basic Research under grant No. 09-08-00888.

REFERENCES

[1]. Tabakoff, W. & Hamed, A. Aerodynamic effect on erosion in turbomachinery. *Proc. JSME and ASME 1977 Joint Gas Turbine Congress*. Tokyo, Japan, pp. 574–581 (1977).

[2]. Stepanov, G.Yu. *Hydrodynamics of cascades of turbomachines*. Moscow, FIZMATLIT (1962). [in Russian]

[3]. Hussein, M.F. & Tabakoff, W. Calculation of particle trajectoties in a stationary two-dimensional cascade. *Dept. of Aero. Engng.* TR 72-27, Unicercity of Cincinnatti, AD-764267 (1972).

[4]. Hussein, M.F., Tabakoff, W. Dynamic behavior of solid particles suspended by polluted flow in a turbine cascade. *J. Aircraft*, Vol. 10, No. 7, pp. 434–440 (1973).

[5]. Tsirkunov, Yu.M. Gas-particle flows around bodies – key problems, modeling and numerical analysis. *Proc. Fourth International Conference on Multiphase Flow* (Ed.: E. Michaelides), New Orleans, LA, USA. CD-ROM ICMF'2001, paper No. 607, 31 p. (2001).

[6]. Anderson, D.A., Tannehill, J.C. and Pletcher, R.H. *Computational Fluid Mechnics and Heat Transfer*, Hemisphere Publ. Corp., New York (1984).

[7]. Tsirkunov, Yu.M., Panfilov, S.V. and Klychnikov, M.B. Semiempirical model of impact interaction of a disperse impurity particle with a surface in a gas suspension flow, *J. Engng. Physics and Thermophysics*, Vol. 67(5-6), pp. 1018–1025 (1994).

[8]. Tsirkunov, Yu., & Panfilov, S. Particle scattering in particle–wall collisions: the combined effect of the particle nonsphericity and the wall roughness. *Proc. 6th International Conference on Multiphase Flow* (Ed.: M. Sommerfeld), Lepzig, Germany. CD-ROM ICMF'2007, paper No. S2TueA15, 10 p. (2007).

[9]. Panfilov, S.V., & Tsirkunov, Yu.M. Scattering of non-spherical particles rebounding from a smooth and a rough surface in a high-speed gas–particle flow. *J. Applied Mech. and Techn. Physics*, Vol. 49, No. 2, pp. 222–230 (2008).

[10]. Henderson, Ch. B. Drag coefficient of spheres in continuum and rarefied flows. *AIAA J.*, Vol. 14, No. 6, pp. 707–708 (1976).

[11]. Rubinow, S.I. & Keller, J.B. The transverse force on a spinning sphere moving in a viscous fluid. *J. Fluid Mech*. 11, 447–459 (1961).

[12]. Oesterle, B. & Bui Dinh, T. Experiments on the lift of a spinning sphere in a range of intermediate Reynolds numbers. *Experim. in Fluids*. 25, 16–22 (1998).

[13]. Dennis, S.R.C., Singh, S.N., and Ingham, D.B. The steady flow due to a rotating sphere at low and moderate Reynolds numbers. *J. Fluid Mech*., 101, 257–279 (1980).

[14]. Roe, P.L. Approximate Riemann solvers, parameter vector and difference schemes. *J. Comput. Phys*., Vol. 43, No. 2, pp. 357–372 (1981).

[15]. Yee, H.C. & Harten, A. Implicit TVD schemes for hyperbolic conservation laws in curvilinear coordinates. *AIAA J*., Vol. 25, No. 2, pp. 266–274 (1987).

[16]. Romanyuk, D.A. & Tsirkunov, Yu.M. Numerical simulation of two-phase gas–particle flow through an inlet stage "rotor–stator" of a turbomachine. *Mathematical modelling* (2009) (in press). [in Russian]